

First-principles study of co-adsorption behavior of O_2 and CO_2 molecules on δ-Pu(100) surface

Chun-Bao Qi(戚春保), Tao Wang(王涛)†, Ru-Song Li(李如松), Jin-Tao Wang(王金涛), Ming-Ao Qin(秦铭澳), and Si-Hao Tao(陶思昊)

Citation: Chin. Phys. B, 2021, 30 (**2**): 026601. DOI: 10.1088/1674-1056/abc158
Journal homepage: http://cpb.iphy.ac.cn; http://iopscience.iop.org/cpb

What follows is a list of articles you may be interested in

Beryllium carbide as diffusion barrier against Cu: First-principles study

Hua-Liang Cao(曹华亮), Xin-Lu Cheng(程新路), Hong Zhang(张红)
Chin. Phys. B, 2020, 29 (**1**): 016601. DOI: 10.1088/1674-1056/ab593e

Diffusion behavior of helium in titanium and the effect of grain boundaries revealed by molecular dynamics simulation

Gui-Jun Cheng(程贵钧), Bao-Qin Fu(付宝勤), Qing Hou(侯氢), Xiao-Song Zhou(周晓松), Jun Wang(汪俊)
Chin. Phys. B, 2016, 25 (**7**): 076602. DOI: 10.1088/1674-1056/25/7/076602

An analytical model of thermal mechanical stress induced by through silicon via

Dong Gang, Shi Tao, Zhao Ying-Bo, Yang Yin-Tang
Chin. Phys. B, 2015, 24 (**5**): 056601. DOI: 10.1088/1674-1056/24/5/056601

Theoretical prediction of ion conductivity in solid state HfO_2

Zhang Wei, Chen Wen-Zhou, Sun Jiu-Yu, Jiang Zhen-Yi
Chin. Phys. B, 2013, 22 (**1**): 016601. DOI: 10.1088/1674-1056/22/1/016601

First-principles study of co-adsorption behavior of O_2 and CO_2 molecules on δ-Pu(100) surface

Chun-Bao Qi(戚春保)[1], Tao Wang(王涛)[1,†], Ru-Song Li(李如松)[2], Jin-Tao Wang(王金涛)[1], Ming-Ao Qin(秦铭澳)[1], and Si-Hao Tao(陶思昊)[1]

[1] *Xi'an Research Institute of High Technology, Xi'an* 710025, *China*
[2] *Xi'an Jiaotong University, Xi'an* 710049, *China*

(Received 15 August 2020; revised manuscript received 12 October 2020; accepted manuscript online 15 October 2020)

First principles calculation is performed to study the co-adsorption behaviors of O_2 and CO_2 on δ-Pu(100) surface by using a slab model within the framework of density functional theory (DFT). The results demonstrate that the most favorable co-adsorption configurations are T_v-C_4O_7 and T_{p1}-C_2O_8, with adsorption energy of -17.296 eV and -23.131 eV for CO_2-based and O_2-based system, respectively. The C and O atoms mainly interact with the Pu surface atoms. Furthermore, the chemical bonding between C/O and Pu atom is mainly of ionic state, and the reaction mechanism is that C 2s, C 2p, O 2s, and O 2p orbitals overlap and hybridize with Pu 6p, Pu 6d, and Pu 5f orbital, resulting in the occurrence of new band structure. The adsorption and dissociation of CO_2 molecule are obviously promoted by preferentially occupying adsorbed O atoms, therefore, a potential CO_2 protection mechanism for plutonium-based materials is that in CO_2 molecule there occurs complete dissociation of CO_2 $\rightarrow$C+O+O, then the dissociated C atom combines with O atom from O_2 dissociation and produces CO, which will inhibit the O_2 from further oxidizing Pu surface, and slow down the corrosion rate of plutonium-based materials.

Keywords: adsorption energy, density functional theory, electron density, reaction mechanism

PACS: 66.30.–h, 65.40.gh, 68.35.–p, 71.15.Mb **DOI:** 10.1088/1674-1056/abc158

1. Introduction

Plutonium, one of the most complex elements in the periodic table, which is on the boundary between the light actinide elements (Th to Pu) with itinerant 5f electrons and heavy actinide elements (Am and later elements) with localized 5f electrons. Elemental Pu and its alloys and compounds are widely used in the nuclear engineering, *e.g.*, the nuclear devices, nuclear reactor, and aerospace fields. In principle, the more localized 5f electrons in Pu-based materials will produce many anomalous physical properties,[1,2] such as the three-peak structures in the photoemission spectra (PES), the negative thermal expansion coefficient in Pu–Ga alloy, and the abnormal magnetic properties, as compared with its neighboring element (U) in the periodic table. From the chemist's viewpoint, additionally, Pu is very active in the atmosphere environment, and is readily to react with almost ordinary molecules in the ambient condition during purification, storage, and usage of Pu-based materials. Energetically, PuO, Pu_2O_3, and PuO_2 are the basic products of plutonium oxidation,[3–6] which poses a great challenge for the long-term storage and protection of plutonium-based materials. In fact, adsorption and dissociation behaviors of the ordinary gaseous molecules, including CO_2 and O_2 considered in this work, on plutonium surface are essential processes for hydrogenation and oxidation corrosion. As a consequence, it is significant to study the adsorption and dissociation of active gases on the plutonium surface in order to understand in depth the corrosion and anti-corrosion mechanisms of Pu-based materials. As a matter of fact, scare direct experimental observation is conducted on Pu-based materials due to its strong chemical activity, radioactivity, and toxicity. For this reason, theoretical work might be an appropriate candidate for studying the adsorption and dissociation behaviors of gas molecules on plutonium surface.

In recent years, there have also been some reports on theoretical researches. Eriksson and Cox[7] calculated the δ-Pu(100) surface under non-magnetic conditions by the surface linear muffin-tin orbit (FLMTO) method. The results showed that the 5f band narrowed, the bonding ability decreased and the surface lattice constant expanded. Huda and Ray[8–11] successively studied the adsorption behaviors of hydrogen, oxygen atoms, and hydrogen and oxygen molecules on the δ-Pu surface by using density functional theory (DFT) and Dmol3 program, showing that the 5f electron localization intensity of δ-Pu(111) surface was stronger than that of δ-Pu(100) surface. On the other hand, Li *et al.*[12,13] studied the surface geometry and electronic structure of δ-Pu monolayer by the full potential linear conjugate plane wave method (FLAPW). The results indicated the degree of localization of 5f electrons on (100) surface was stronger than that on (111) surface, which was exactly opposite to Huda's result. Atta-Fynn and Ray[14,15] studied the adsorption of C, N, O atoms on δ-Pu(111) sur-

†Corresponding author. E-mail: wtao009@163.com

© 2021 Chinese Physical Society and IOP Publishing Ltd

face and the effect of surface relaxation on adsorption by the FLAPW method. Meng *et al.*[16] investigated the adsorption and dissociation behavior of CO_2 molecule on Pu(100) surface by the modified Perdew–Burke–Emzerh (PBE) method based on the generalized gradient density functional theory and Dmol3 program. The calculated dissociation energy barrier of CO_2 →CO+O was 0.66 eV and the dissociation adsorption energy was 2.65 eV. Luo *et al.*[17] studied the adsorption of CO molecule on Pu(100) surface by DFT and Dmol3 program. The results demonstrated that the dissociation energy barrier of CO molecule adsorbing on obliquely hollow was relatively small (0.280 eV). Wang and Ray[18] used GGA-DFT, DMOL3, and WIEN2k to study the adsorption of CO_2 on nano-layer of α-Pu(020) surface. The results revealed that the completely dissociated configuration (C+O+O) had the strongest surface binding (7.94 eV), followed by partial dissociated configuration (CO+O) and CO_2 molecular configuration (5.18 eV and 1.90 eV respectively). Atta-Fynn and Ray[19] used the *ab initio* calculation method within the framework of DFT and Dmol3 program to study the adsorption and dissociation behavior of CO_2 molecule on δ-Pu(111) surface. The results indicated that the fully dissociated configuration (C+O+O) showed the strongest binding to the surface (7.92 eV), followed by the partially dissociated configuration CO+O (5.08 eV), with the lowest binding energy of CO_2 molecule adsorption (2.35 eV). Wei *et al.*[20] used the GGA of periodic DFT and DMOL3 program to study the adsorption behavior of O atom on δ-Pu(111) surface. The results demonstrated that the adsorption of O atom on δ-Pu(111) surface belonged to strong chemical reaction. Guo *et al.*[21] studied the adsorption behavior of O_2 molecule on δ-Pu(100) surface by DMOL3 program, DFT and periodic plate model. The results showed that O dissociative adsorption was found to be energetically more favorable than molecular adsorption and the dissociative oxygen atom preferred adsorption on the center site. Li *et al.*[22] calculated the electronic structure of Pu compounds by using DFT. The results indicated that PuH_2 compound has the metallic character, and the Pu–H bonds in PuH_3 compound, Pu–O bond in PuO compound, Pu–N bond in PuN compound and Pu–S bond compound were essentially ionic in character. The Pu–C bond in PuC compound, Pu–O bond in Pu_2O_3 compound and Pu–O bond in PuO_2 compound were covalent in character. One can see that the predecessors mostly used DMOL3 program to study the adsorption and dissociation of C, N, O, O_2, and CO_2 on Pu surface and the results may be controversial, however, the VASP program has not been reported publicly to perform such researches. In the VASP program used is PAW pseudopotential, belonging to density functional method, which has the faster calculation speed and higher efficiency with the adjustable parameters than the DMOL3 program in which used is DSPP basic, thus, we select the VASP program to perform calculation in this paper.

To the best of our knowledge, the previous reports paid much attention to the adsorption of individual molecules, however, there have existed few researches on the co-adsorption process, such as CO_2 and O_2 co-adsorption addressed in this work, which might be more important from the viewpoint of practical applications. On the other hand, mechanically, δ-phase plutonium is more ductile and readily-processing than its another allotrope, such as the room-temperature α phase. Therefore, we plan to perform a first principles calculation for the co-adsorption of O_2 and CO_2 on a representative face of δ-phase plutonium, *i.e.*, δ-Pu(100) surface. Specially, we focus on the stable adsorption configuration, the change of electronic structure, the adsorption energy as well as the charge transfer induced by co-adsorption, which might give a new perspective of the corrosion and anti-corrosion mechanisms of O_2 and CO_2 with δ-Pu(100) surface.

2. Computational details

2.1. Methods

All calculations are implemented within Vienna *ab-initio* simulation package (VASP5.4.4)[23] on the basis of density functional theory (DFT).[24,25] It uses projection augmented wave (PAW)[26,27] pseudopotential method for first-principles calculation, which is an efficient plane wave pseudopotential package and widely used in the calculation of electronic structures.[28–30] Generalized gradient approximation (GGA) in the form of Perdew–Burke–Ernzerhof (PBE) exchange–correlation potential is used to approximate the electron exchange correlation interactions.[31,32] There are 16, 4, and 6 valence electrons in the outer shells for Pu ion ($6s^2 6p^6 5f^6 7s^2$), C ion ($2s^2 2p^2$), and O ion ($2s^2 2p^4$), respectively. Monkhorst–Pack (MP)[33] scheme is used to sample data inside the irreducible Brillouin-zone. Spin polarization effect is considered in all calculations.

The ion position, cell shape and cell volume are changed when the δ-Pu cell is optimized with a $7 \times 7 \times 7$ k-point mesh used. The lower two layers are fixed and the upper two layers are released for optimization with the shape and volume unchanged when the δ-Pu(100) 4-layer slab is optimized. The 4 layers of Pu atoms are fixed, and O_2 and CO_2 molecules[16] on the optimized surface are released when the O_2 and CO_2 adsorption system is optimized. The k-point mesh of δ-Pu(100) surface and adsorption system are both set to be $5 \times 5 \times 1$. The proportional coefficient of acting force is 0.5 and the N-th-order Methfessel–Paxton method is applied to the optimization of the δ-Pu unit cell, its surface and adsorption system. For all optimization calculations, a plane-wave cut off energy of 450 eV is adopted to insure that the total energy of all structures is converged within 0.5 meV/atom, and the conjugate

gradient (CG)[34] method of Hellman–Feynman force is applied to the ion optimization. The convergence criterion of atomic force is 10^{-2} eV/Å and the energy convergence criterion is 10^{-4} eV, respectively. The total energy is acquired by one-step self-consistent calculation on the basis of the optimized model. The wave function, charge density, work function and charge transfer of O_2 molecule, CO_2 molecule, δ-Pu(100) surface and adsorption system are also addressed in this paper.

The surface energy, E_{sur}, is then obtained from the following equation:

$$E_{sur} = (E_{slab} - NE_{bulk})/2A, \quad (1)$$

where A is the cross-sectional area of the slab, E_{slab} is the total energy of the slab, N is the number of Pu atoms in the slab, and E_{bulk} is the energy of a single Pu atom in the bulk.

The co-adsorption energy of O_2 and CO_2 molecules on the δ-Pu(100) surface is given by

$$E_{co-ads} = E_{[O_2\&CO_2/Pu(100)]} - E_{O_2} - E_{CO_2} - E_{Pu(100)}, \quad (2)$$

where $E_{[O_2\&CO_2/Pu(100)]}$ is the total energy of the system after co-adsorption, E_{O_2} is the energy of the O_2 molecule, E_{CO_2} is the energy of the CO_2 molecule, and $E_{Pu(100)}$ is the energy of the δ-Pu(100) surface. The energy of O_2 and CO_2 molecules are the ground state energy under the same calculation method. For negative adsorption energy, the structural stability is increased by adsorption. Moreover, the less the adsorption energy, the more stable the structure is.

2.2. Models

2.2.1. Surface model

The crystal structure of metallic δ-Pu is facecentered cubic (fcc) with the space group code of Fm-3m. The optimized Pu crystal lattice is 4.772 Å, which is in good agreement with the experimental value of 4.637 Å[9] within an error rate of 2.9%. The optimized O–O bond length is 1.235 Å, which is consistent with an experimental value of 1.208 Å within an error rate of 2.6%.[35] The optimized C–O bond length is 1.177 Å, which is consistent with the experimental value of 1.162 Å with an error rate of 1.3%.[36] From the test results of surface energy convergence and references,[16,17] we find that the E_{sur} difference between $p(3\times3)$ and $p(2\times3)$, and between $p(2\times3)$ and $p(2\times2)$ slabs are 0.007 eV·Å^{-2} and 0.043 eV·Å^{-2}, respectively, and that the differences are negligibly small and will not affect the main conclusion. Therefore, 4 layers of Pu atomic layer crystals (slab) of $p(2\times2)$ are established within an optimized δ-Pu unit cell to simulate the δ-Pu(100) surface. A vacuum layer with 15 Å in thickness[37] is set on the z axis of the δ-Pu(100) surface to ensure that the interaction between adjacent layers is negligibly small. The lattice constants of the supercell are $a = b = 6.7488$ Å and $c = 22.1581$ Å, respectively, and the slab model is shown in Figs. 1(a) and 1(b), in which the z coordinate and layer spacing between two Pu atoms decrease on the surface. Figure 1(c) shows the adsorption sites on the δ-Pu(100) surface.

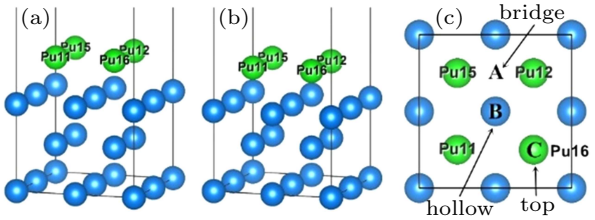


Fig. 1. Structure model of δ-Pu(100) slab and top view of three adsorption sites on surface (Pu atoms on surface and on other three layers are green- and blue-colored, respectively): (a) before optimization, (b) after optimizations, and (c) top view; A: bridge site, B: hollow sites, and C: top site.

2.2.2. Co-adsorption models

The adsorption model contains sixteen Pu atoms and one O_2 and one CO_2 molecule with a total of 21 atoms. Moreover, the monolayer adsorption coverage (θ) of O_2 and CO_2 is 0.25. According to our previous work,[38,39] the best adsorption configuration of O_2 and CO_2 on δ-Pu(100) surface is bridge parallel 2 and hollow parallel 1, respectively. Consequently, the co-adsorption behavior of O_2 and CO_2 on δ-Pu(100) surface is investigated by studying the co-adsorption configuration of CO_2 and O_2 when they occupy the individual best adsorption configuration, and the following models are established.

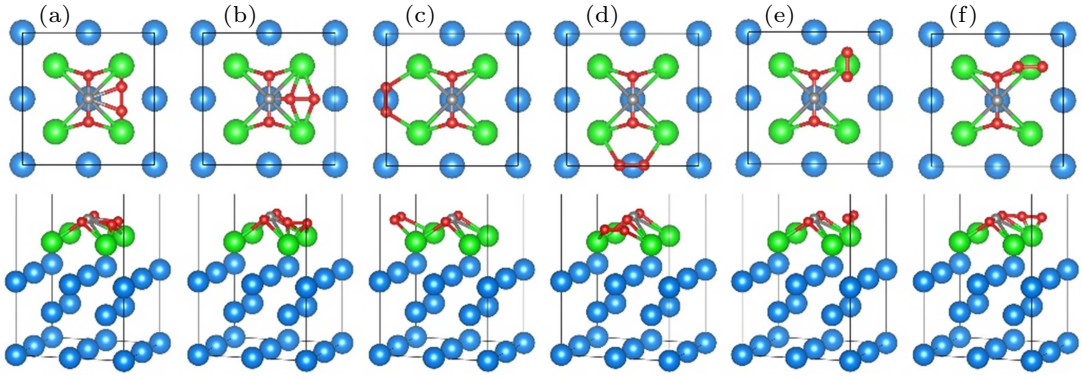


Fig. 2. Top and side views of different models for O_2 adsorption on the δ-Pu(100) surface in CO_2-based case (Pu on surface, Pu, C, and O atoms on other three layers are green-, blue-, grey-, and red-colored, respectively): (a) bridge parallel, (b) bridge vertical, (c) hollow parallel, (d) hollow vertical, (e) top parallels, and (f) top vertical.

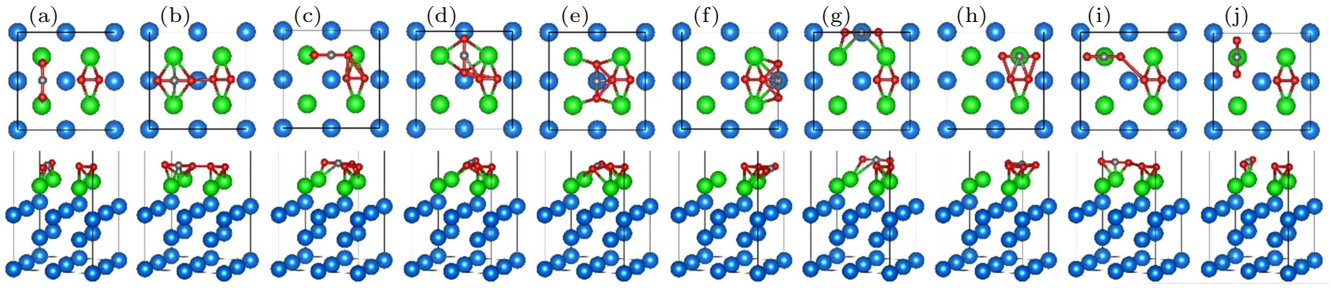


Fig. 3. Top and side views of different models for CO_2 adsorption on δ-Pu(100) surface in O_2-based case (Pu on surface, Pu, C, and O atoms on other three layers are green-, blue-, grey-, and red-colored, respectively): (a) bridge vertical 1, (b) bridge parallel 1, (c) bridge parallel 2, (d) bridge vertical 2, (e) hollow vertical 1, (f) hollow vertical 2, (g) hollow parallel, (h) top parallel 1, (i) top parallel 2, and (j) top vertical.

(i) O_2 molecules are placed at the top, bridge and hollow sites to establish a co-adsorption model when CO_2 is at the best adsorption configuration (denoted as CO_2-based). Furthermore, each site involving with one of two cases: O_2 approaches parallelly or vertically to CO_2, for this reason, there are six co-adsorption models as shown in Fig. 2. (ii) Similarly, CO_2 molecules are placed at three sites to establish a co-adsorption model when O_2 molecule is in the best adsorption configuration (abbreviated as O_2-based), and there are 10 adsorption models as shown in Fig. 3.

3. Results and discussion

3.1. Adsorption configurations and energy

Six adsorption models in CO_2-based case and ten co-adsorption models in O_2-based case are optimized. We define configurations in accordance with the adsorption positions occupied by O_2 and the bonding numbers of C and O atoms with Pu atoms adjacent to the surface layer in CO_2-based case in order to distinguish them. For example, B_p-C_4O_6 indicates that the adsorption state of O_2 is bridge parallel and C and O atoms are bonded with 4 and 6 Pu atoms adjacent to the surface layer, respectively. There are six adsorption configurations as shown in Fig. 4. Similarly, we use the adsorption sites occupied by CO_2 and the bonding numbers of C and O atoms with Pu atoms adjacent to the surface layer to define the configuration in the O_2-based case. For instance, H_{v1}-C_4O_8 means that the adsorption state of CO_2 is hollow vertical 1 and C and O atoms are bonded with 4 and 8 Pu atoms adjacent to the surface layer, respectively. As a result, ten adsorption configurations are plotted in Fig. 5. The optimized geometrical and energy parameters of O_2 and CO_2 co-adsorption on the δ-Pu(100) surface are listed in Table 1.

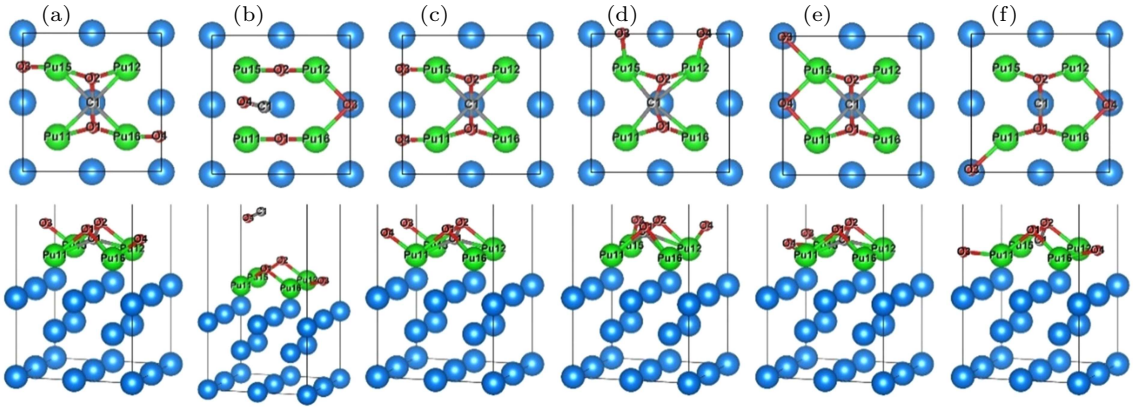


Fig. 4. Top and side views of optimized structures for O_2 adsorption on δ-Pu(100) surface in CO_2-based case (Pu on surface, Pu, C, and O atoms on other three layers are green-, blue-, grey-, and red-colored, respectively): (a) B_p-C_4O_6, (b) B_v-C_0O_6, (c) H_p-C_4O_6, (d) Hv-C_4O_6, (e) Tp-C_4O_7, and (f) T_v-C_4O_7; B_p: bridge parallel, B_v: bridge vertical, H_p: hollow parallel, H_v: hollow vertical, T_p: top parallel, and T_v: top vertical.

According to the data in Fig. 4 and Table 1, in the CO_2-based case, from the viewpoint of CO bond length and θ_{O-C-O}, CO_2 molecules are adsorbed at C-terminated configurations except the B_v-CO_6 configuration, and the CO bond length is in a range of 1.332 Å–1.422 Å, which is significantly longer than that of gaseous CO_2 molecule (1.177 Å). Obviously, CO_2 molecule presents in-plane bending after adsorption, and the bond angle of θ_{O-C-O} decreases from 180° to 114.66°–119.57°, among which T_v-C_4O_7 adsorption configuration has the longest C–O bond length (1.422 Å) and the smallest θ_{O-C-O} (114.66°), showing that T_v–C_4O_7 configuration is the most stable. Furthermore, from the viewpoint of atomic position after adsorption, the distances between two oxygen atoms in six configurations increase to more than 3.0 Å, consequently, the O–O bond is completely broken and dissociated into two oxygen atoms adsorbed on the δ-Pu(100) surface, namely, the spontaneous dissociation happens to O_2 by forming ionic bond with Pu surface atoms, which can

be seen from the charge-density difference in Figs. 8(a) and 9(a). The adsorbed O atoms are located at bridge position in the three configurations of B_p-C_4O_6, H_p-C_4O_6, and H_v-C_4O_6, and O atoms occupy the hollow sites in B_v-CO_6, T_p-C_4O_7, and T_v-C_4O_7 configurations after O_2 has dissociated, showing that the O atoms preferentially occupy the hollow and bridge sites after co-adsorption has taken place. The co-adsorption energy of the six CO_2-based adsorption configurations are −1.773 eV, −11.544 eV, −8.558 eV, −5.149 eV, −7.143 eV, and −17.296 eV, respectively, indicating that the co-adsorption stability is order as T_v-C_4O_7 > B_v-CO_6 > H_p-C_4O_6 > T_p-C_4O_7 > H_v-C_4O_6 > B_p-C_4O_6, the absolute value of six co-adsorption sites are obviously larger than 40 kJ/mol, revealing that the co-adsorptions belong to strong chemical adsorption, T_v-C_4O_7 configuration has the smallest adsorption energy, *i.e.*, the most stable chemisorption site.

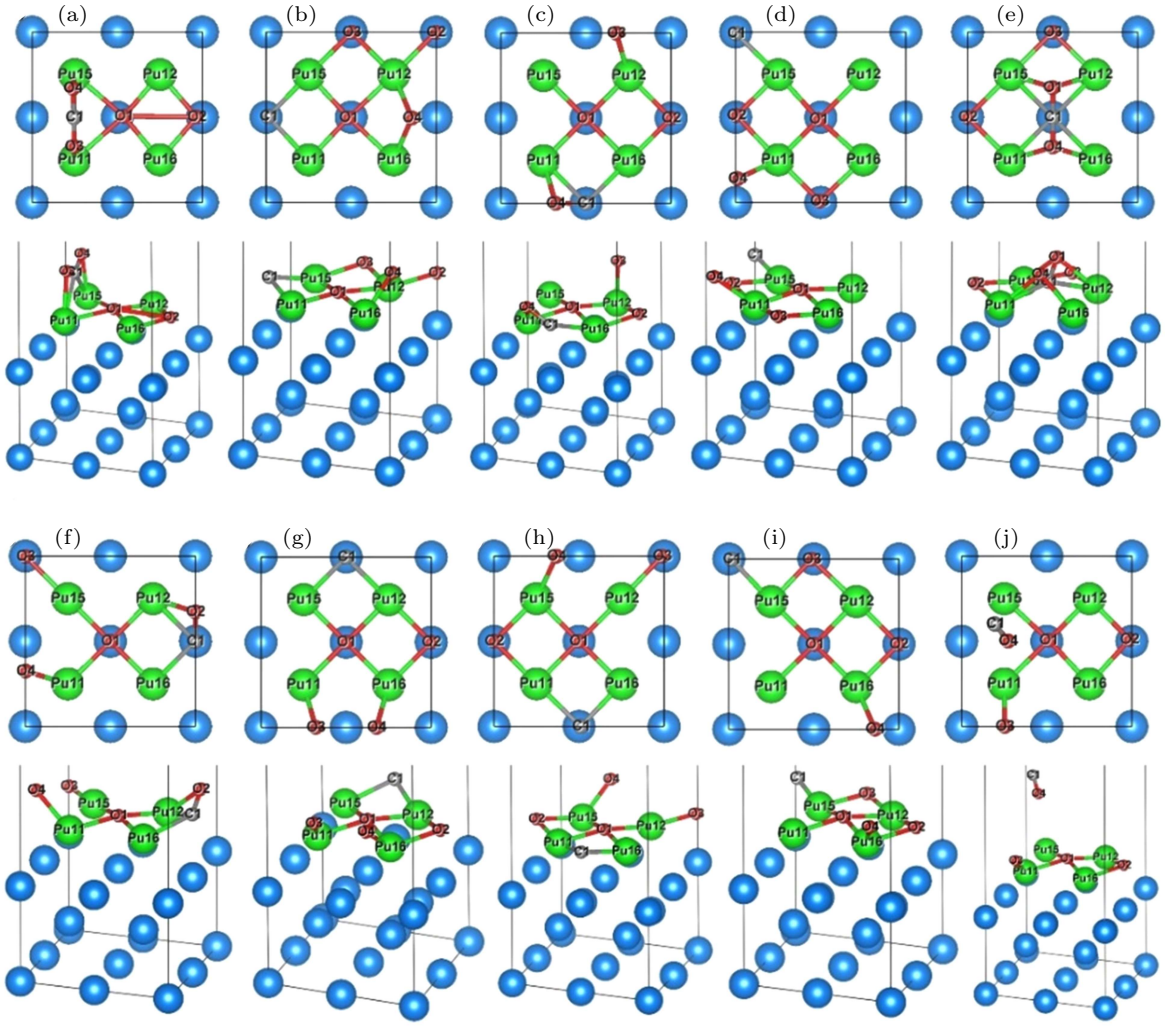


Fig. 5. Top and side views of optimized structures for CO_2 adsorption on δ-Pu(100) surface in O_2-based case (Pu on surface, Pu, C, and O atoms on other three layers are green-, blue-, grey-, and red-colored, respectively): (a) B_{v1}-C_2O_8, (b) B_{p1}-C_1O_9, (c) B_{p2}-C_2O_8, (d) B_{v2}-C_1O_9, (e) H_{v1}-C_4O_8, (f) H_{v2}-C_2O_7, (g) H_p-C_2O_6, (h) T_{p1}-C_2O_8, (i) T_{p2}-C_1O_9, and (j) T_v-C_0O_7; B_{v1}: bridge vertical 1, B_{p1}: bridge parallel 1, B_{p2}: bridge parallel 2, B_{v2}: bridge vertical 2, H_{v1}: hollow vertical 1, H_{v2}: hollow vertical 2, H_p: hollow parallel, T_{p1}: top parallel 1, T_{p2}: top parallel 2, and T_v: top vertical.

Combination of the data in Fig. 5 and Table 1 shows that for O_2-based co-adsorption, from the viewpoint of CO bond length and adsorption configuration, only in B_{v1}-C_2O_8 configuration (Fig. 5(a)), CO_2 molecule is bent and not dissociated, and at this time θ_{O-C-O} is 131.62° and C-O bond length is 1.270 Å. However, CO_2 is partially or completely dissociated in the other nine configurations. The CO_2 molecule presents the partial dissociation of CO_2 →CO+O and O_2 is also dissociated into H_{v1}-C_4O_8 configuration, the dissociated O1 atom (Fig. 5(e)) combines with CO and produce a bent CO_2 molecule adsorbed on the δ-Pu(100) surface, in which the θ_{O-C-O} is 114.63° and C–O bond length is 1.399 Å. In the B_{p2}-C_2O_8 and T_v-CO_7 configurations, for partial dissociation of CO_2 molecules (CO_2 →CO+O), the C–O bond lengths are 1.419 Å and 1.144 Å, respectively. However, the dissociated CO is far away from the δ-Pu(100) surface in T_v-CO_7 configuration (Fig. 5(j)). In sharp contrast, in B_{p1}-C_1O_9, B_{v2}-C_1O_9, H_{v2}-C_2O_7, H_p-C_2O_6, T_{p1}-C_2O_8, and T_{p1}-C_1O_9 configurations, CO_2 molecules completely dissociate into C+O+O, and C atom combines with the O_2 atom dissociated (Fig. 5(f)) from O_2 and thus producing CO with a C–O bond length of 1.393 Å in H_{v2}-C_2O_7 configuration. In the other five configu-

rations, O_2 and CO_2 molecules are dissociated completely into C and O atoms stably adsorbed on the δ-Pu(100) surface. The distance between two O atoms in O_2 increases from 1.235 Å to more than 3.0 Å and the O–O bond is completely broken. Besides, the dissociated O atoms and the dissociated O3 atom from CO_2 molecule are all preferentially adsorbed on the hollow site. Obviously, it is should be noted that the preferentially occupying adsorption of O atoms can promote the adsorption and dissociation of CO_2 molecules. The co-adsorption energy of ten O_2-based adsorption configurations are in a range of −23.131 eV to −3.213 eV, demonstrating that the adsorption stability is in the order of T_{p1}-C_2O_8 > B_{v2}-C_1O_9>T_v-CO_7 > B_{p2}-C_2O_8>T_{p2}-C_1O_9 > B_{p1}-C_1O_9>B_{v1}-C_2O_8 > H_p-C_2O_6 > H_{v1}-C_4O_8 > H_{v2}-C_2O_7, the absolute values of sixteen co-adsorption sites are all obviously larger than 40 kJ/mol, revealing that the co-adsorptions belong to strong chemical adsorption. Moreover, the T_{p1}-C_2O_8 configuration has the smallest adsorption energy, *i.e.*, the most stable chemisorption site.

Table 1. Optimized geometrical and energy parameters of O_2 and CO_2 co-adsorption on δ-Pu(100) surface. d denotes bond length between C and O atoms, d_{C-Pu} or d_{O-Pu} is average bond distance between the adsorbed C or O atoms and neighbor surface Pu atoms, θ_{O-C-O} is OCO bond angle, h_{C-S} or h_{O-S} is average adsorption height of C or O atoms with respect to the first layer, and E_{co-ads} is co-adsorption energy.

Base	Configuration	Bond	d (Å)	d_{C-Pu} (Å)	d_{O-Pu} (Å)	θ_{O-C-O} (°)	h_{C-S} (Å)	h_{O-S} (Å)	E_{co-ads} (eV)
CO_2	B_p-C_4O_6	C–$O_{1/2}$	1.391	2.498	2.190	117.64	0.738	1.306	–1.773
	B_v-CO_6	C–O_4	1.144		2.172	–	4.637	1.699	–11.544
	H_p-C_4O_6	C–$O_{1/2}$	1.398	2.495	2.162	117.60	0.728	1.302	–8.558
	H_v-C_4O_6	C–$O_{1/2}$	1.332	2.651	2.264	119.57	1.106	1.254	–5.149
	T_p-C_4O_7	C–$O_{1/2}$	1.420	2.478	2.293	114.87	0.667	0.872	–7.143
	T_v-C_4O_7	C–$O_{1/2}$	1.422	2.474	2.307	114.66	0.653	0.873	–17.296
O_2	B_{v1}-C_2O_8	C–$O_{3/4}$	1.270	2.506	2.359	131.62	1.853	1.278	–9.756
	B_{p1}-C_1O_9			2.376	2.377	–	0.488	0.549	–13.512
	B_{p2}-C_2O_8	C–O_4	1.419	2.482	2.370	–	0.692	0.869	–15.768
	B_{v2}-C_1O_9			2.383	2.378	–	0.409	0.551	–19.868
	H_{v1}-C_4O_8	C–O1/4	1.399	2.491	2.344	114.63	0.714	0.805	–5.825
	H_{v2}-C_2O_7	C–O_2	1.393	2.485	2.363	–	0.712	0.804	–3.213
	H_p-C_2O_6			2.478	2.360	–	0.680	0.871	–6.845
	T_{p1}-C_2O_8			2.414	2.383	–	0.372	0.544	–23.131
	T_{p2}-C_1O_9			2.362	2.394	–	0.524	0.565	–13.705
	T_v-CO_7	C–O_4	1.144	–	2.371	–	4.614	1.437	–19.144

From the viewpoint of bonds binding, the average CPu bond lengths between C atoms and Pu surface atoms are in a range of 2.474 Å–2.651 Å for CO_2-based systems, and the average C-Pu bond lengths are in a range of 2.362 Å–2.506 Å for O_2-based systems, which are close to the bond lengths between C atoms and Pu atoms in carbide crystals (PuC: 2.4620 Å; PuC_2: 2.2819 Å).[40] The average O–Pu bond lengths between O atom and neighboring Pu atom are in a range of 2.162 Å–2.307 Å for CO_2-based systems, and the average O–Pu bond lengths are in a range of 2.359 Å–2.394 Å for O_2-based systems, which is slightly larger than that in Pu oxide crystal (PuO: 1.830 Å; PuO_2: 1.810 Å),[41,42] indicating that O_2 and CO_2 molecules are stably co-adsorbed on δ-Pu (100) surface by strong chemical bonding between C/O atoms and Pu atoms. To this end, the C atoms dissociated from CO_2 combine with O atoms dissociated from O_2 to produce CO in O_2-based case, which will inhibit the O atoms from further oxidizing Pu surface,[43] and slow down the corrosion rate of plutonium-based materials and protect them, which is the anti-corrosion mechanism of CO_2 for plutonium surface.

3.2. Bader charge distribution

In principle, the atom loses electrons and the valence is positive when the corresponding net charge is negative, on the contrary, the atom gains electrons and the valence is negative when the corresponding net charge is positive. Charge transfer occurs among C, O, and Pu atoms originating from O_2 and CO_2 co-adsorption on the δ-Pu(100) surface. In order to clearly elucidate the interaction among O_2, CO_2 molecules and Pu surface atoms, Bader charge distribution[44] of (O_2&CO_2)/δ-Pu(100) co-adsorption system are calculated as listed in Table 2. The $q_{substance}$ in Table 2 is defined as follows:

$$q_{atom} = q_{Bader} - q_{valence}, \tag{3}$$

where q_{atom}, q_{Bader}, and $q_{valence}$ are the net charge, Bader charge, and valence electron of atom, respectively. Figures 6 and 7 show the charge distribution of ions in CO_2-based and O_2-based co-adsorption system, respectively.

As shown in Table 2, from the perspective of charge transfer, CO_2 molecule and two O atoms are in different charge states (in a range of 3.4654e–4.7718e) in the CO_2-based case, and the q_{1st} changes obviously from −0.4220e to −4.4978e–3.6621e, while q_{2nd} changes little from 0.5124e to −0.4217e–0.6702e. The q_{3rd} changes slightly from 0.2700e to −0.5124e–−0.4823e, the least change appears in the q_{4th} case (from −0.3604e to −0.4627e–−0.2643e).

Table 2. Net charge distribution of (O_2 & CO_2)/δ-Pu(100) co-adsorption system. q_{total} is total net charge number of the C, O_1, O_2, O_3, and O_4 ions, q_{1st}, q_{2nd}, q_{3rd}, and q_{4th} represent total net charge numbers of the first layer to the fourth layer on the δ-Pu(100) surface, respectively. All q's values are in units of e.

Base	Configuration	Atoms					q_{total}	Layers			
		q_C	q_{O_1}	q_{O_2}	q_{O_3}	q_{O_4}		q_{1st}	q_{2nd}	q_{3rd}	q_{4th}
CO_2	free CO_2&O_2	–1.7496	0.8690	0.8806	–0.0430	0.0430	0	–	–	–	–
	free surface	–	–	–	–	–	–	–0.4220	0.5124	0.2700	–0.3604
	B_p-C_4O_6	–0.2583	1.0435	1.0576	1.0551	1.0322	3.9301	–4.2218	0.6251	–0.0224	–0.3109
	B_v-CO_6	–1.1068	1.0937	1.0765	1.2873	1.1147	3.4654	–3.6621	0.4848	0.0135	–0.3016
	H_p-C_4O_6	–0.2264	1.0542	1.0530	1.0351	1.0361	3.9520	–4.2590	0.6702	–0.0386	–0.3246
	H_v-C_4O_6	–0.6599	1.0921	1.0908	1.0088	1.0473	3.5791	–3.8869	0.5905	–0.0185	–0.2643
	T_p-C_4O_7	–0.1746	1.0749	1.0801	1.3021	1.2666	4.5491	–4.4978	–0.0855	0.3372	–0.3028
	T_v-C_4O_7	0.0123	1.0523	1.0173	1.3137	1.3762	4.7718	–4.3698	–0.4217	0.4823	–0.4627
O_2	free O_2&CO_2	–1.7496	–0.0430	0.0430	0.8690	0.8806	0	–	–	–	–
	B_{v1}-C_2O_8	–1.2599	1.1971	1.2125	1.1107	1.1256	3.3860	–3.4615	0.1320	0.2923	–0.3488
	B_{p1}-C_1O_9	0.6743	1.3622	1.3351	1.3464	1.0781	5.7961	–5.0361	–0.8202	0.5668	–0.5067
	B_{p2}-C_2O_8	–0.1444	1.2857	1.2843	1.0568	1.0685	4.5509	–4.1757	–0.3510	0.4514	–0.4756
	B_{v2}-C_1O_9	0.6012	1.2949	1.2315	1.2655	1.1018	5.4948	–5.1051	–0.4285	0.3759	–0.3371
	H_{v1}-C_4O_8	–0.2439	1.0610	1.2823	1.3115	1.0633	4.4743	–4.3396	–0.1380	0.2653	–0.2621
	H_{v2}-C_2O_7	–0.2558	1.2809	1.0620	1.2490	1.0692	4.4053	–4.3099	0.1326	0.0776	–0.3056
	H_p-C_2O_6	–0.1471	1.2717	1.3199	1.0696	1.0691	4.5833	–4.5798	–0.0191	0.3766	–0.3611
	T_{p1}-C_2O_8	0.6385	1.2843	1.3111	1.2706	1.0820	5.5865	–5.1518	–0.4444	0.3459	–0.3363
	T_{p2}-C_1O_9	0.5583	1.3027	1.2877	1.2571	1.0917	5.4974	–5.0792	–0.4905	0.3987	–0.3265
	T_v-CO_7	–1.0762	1.2899	1.2910	1.1665	1.0913	3.7624	–3.8115	0.1396	0.2169	–0.3075

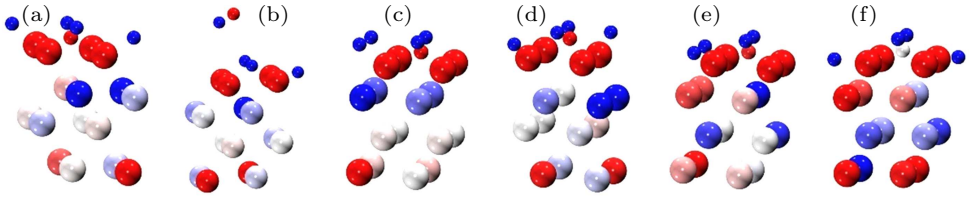


Fig. 6. Charged state of each atom in CO_2-based co-adsorption system, with red- and blue-colored spheres denoting positively and negatively charged atoms, respectively, charge ranging from $-0.20e$ to $+0.20e$. (a) B_p-C_4O_6, (b) B_v-C_0O_6, (c) H_p-C_4O_6, (d) Hv-C_4O_6, (e) Tp-C_4O_7, and (f) T_v-C_4O_7.

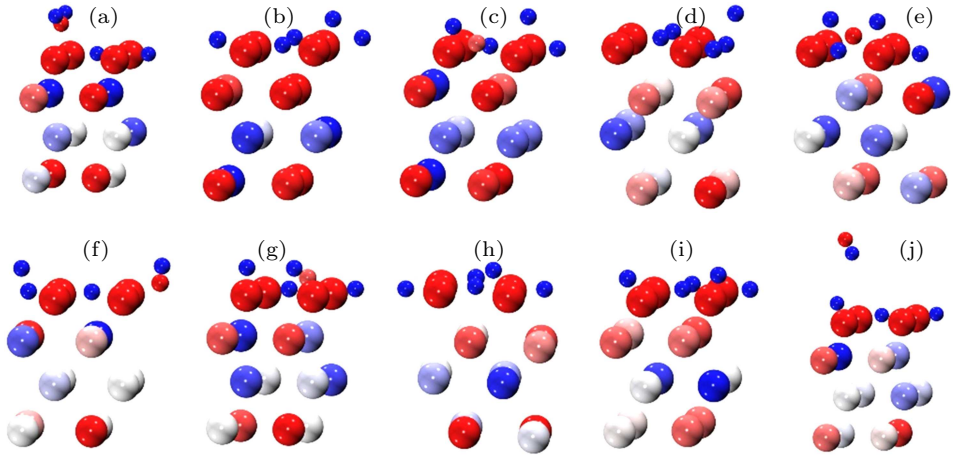


Fig. 7. Charged state of each atom in O_2-based co-adsorption system, with red- and blue-colored spheres denoting positively and negatively charged atoms, respectively, and charge ranging from $-0.20e$ to $+0.20e$. (a) B_{v1}-C_2O_8, (b) B_{p1}-C_1O_9, (c) B_{p2}-C_2O_8, (d) B_{v2}-C_1O_9, (e) H_{v1}-C_4O_8, (f) H_{v2}-C_2O_7, (g) H_p-C_2O_6, (h) T_{p1}-C_2O_8, (i) T_{p2}-C_1O_9, and (j) T_v-C_0O_7.

Similarly, in the O_2-based case, the adsorbed C atoms and four O atoms are charged with 3.3860e–5.7961e, and q_{total} value of B_{p1}-C_1O_9, B_{v2}-C_1O_9, T_{p1}-C_2O_8, and T_{p2}-C_1O_9 sites are 5.7961e, 5.4948e, 5.5865e, and 5.4974e, respectively, in which the adsorbed C atoms are charged with 0.6743e, 0.6012e, 0.6385e, and 0.5583e, respectively, indicating that the valences of C atoms are negative, however, in the other six configurations, the net charges of C atoms are negative and the valence are positive, demonstrating that these four sites react strongly with Pu surface atoms, and the adsorption energy values are −15.768 eV, −19.868 eV, −23.131 eV, and −13.705 eV, respectively, which also establish the strong re-

action in these configurations. The q_{1st} changes remarkably from $-0.4220e$ to $-5.1518e$–$-3.4615e$, the q_{2nd} changes little from $0.5124e$ to $-0.8202e$–$0.1396e$, the q_{3rd} changes slightly from $0.2700e$ to $0.0776e$–$0.5668e$, the least change appears for the q_{4th} case (from $-0.3604e$ to $0.5067e$–$-0.2621e$). All the above-mentioned results demonstrate that charge mainly transfer from surface Pu atoms to C and O atoms, namely, C and O atoms mainly interact with Pu surface atoms, while the interaction with other three layers of Pu atoms is weak.

The transfer charge is $4.7718e$ for the T_v-C_4O_7 site, which is less than that ($5.5865e$) for T_{p1}-C_2O_8 configuration, revealing that the charge transfer and reaction intensity of the latter are stronger than those for the T_{p1}-C_2O_8 configuration. In the CO_2-based case, the q_{total} values of two top sites (T_p-C_4O_7 and T_v-C_4O_7) are $4.5491e$ and $4.7718e$, respectively, which are larger than those of bridge and hollow sites. Therefore, as compared with the hollow and bridge sites, top site is very favorable for charge transfer.

Figures 6 and 7 reflect the charge state of each atom after co-adsorption, one can see that O atoms always gain electrons and are negatively charged, which also hold the C atoms in T_v-C_4O_7, B_{p1}-C_1O_9, B_{v2}-C_1O_9, T_{p1}-C_2O_8, and T_{p2}-C_1O_9 configurations, however, C atoms and Pu surface atoms lose electrons and are positively charged in the other 11 configurations, which are consistent with the results of Table 2.

3.3. Electronic structure analysis

From the viewpoint of the microscopic mechanism, co-adsorption will result in the change of the electronic structure. For exploring the reaction mechanism among O_2, CO_2 molecules, and Pu surface atoms, binding character among the O_2, CO_2 molecules, and Pu surface has been examined by the charge–density difference. For the fully relaxed, minimum total-energy T_v-C_4O_7 and T_{p1}-C_2O_8 configurations in the CO_2-based and O_2-based case, respectively, the charge-density difference is given by

$$\rho = \rho_{[(O_2\ \&\ CO_2)/\delta\text{–Pu}(100)]} - \rho_{(O_2)} - \rho_{(CO_2)} - \rho_{[\delta\text{–Pu}(100)]}, \quad (4)$$

where $\rho_{[(O_2\ \&\ CO_2)/\delta\text{–Pu}(100)]}$, $\rho_{(O_2)}$, $\rho_{(CO_2)}$, and $\rho_{[\delta\text{–Pu}(100)]}$ are charge density of $(O_2\ \&\ CO_2)/\delta$-Pu(100) adsorption system, O_2 molecules, CO_2 molecules, and δ-Pu(100) surface, respectively. The electronic density of states (DOS) of T_v-C_4O_7 and T_{p1}-C_2O_8 sites are calculated. The isosurfaces of charge–density difference between these two configurations are also addressed as shown in Fig. 8. The spatial distribution of charge accumulation and loss are represented by contour lines in the charge-density difference, which can directly determine the bonding condition of ions in the co-adsorption system. Figure 8 clearly shows that the O atoms gain electrons and the charge density increases obviously, while Pu atoms in the surface layer lose electrons and the charge density decreases, which also confirms that the chemical bonding between Pu and O atoms is mainly in ionic state, and the charge accumulation and loss intensity of T_{p1}-C_2O_8 configuration are stronger than those of T_v-C_4O_7 configuration.

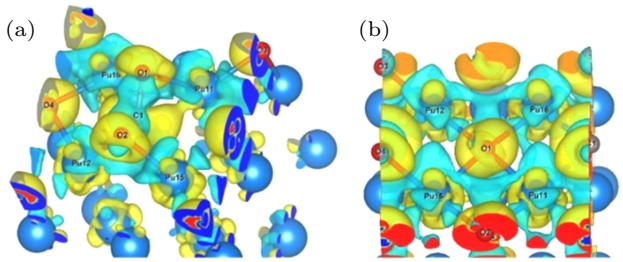


Fig. 8. Isosurfaces of charge–density difference for (a) T_v-C_4O_7 and (b) T_{p1}-C_2O_8 configurations, with yellow and blue colors denoting increase and decrease in charge density, respectively (Isosurfaces level: 0.005 e/Å^3).

In order to clearly demonstrate the chemical state in T_v-C_4O_7 configuration and T_{p1}-C_2O_8 configuration, we plot the two-dimensional (2D) contour isosurfaces of the charge-density difference for C1, O1, O_2 atoms and O1, O_2, O3 atoms along the best planes of (-1 153.66 11.37) and (1 2.14 266.76) in Figs. 9(a) and 9(b), respectively. One can see that C and O atoms are surrounded by electrons, and there is no unpaired electrons between C/O and Pu atoms, demonstrating the ionic chemical bond, which is in good agreement with the three-dimensional (3D) isosurfaces of the charge–density difference in Fig. 8.

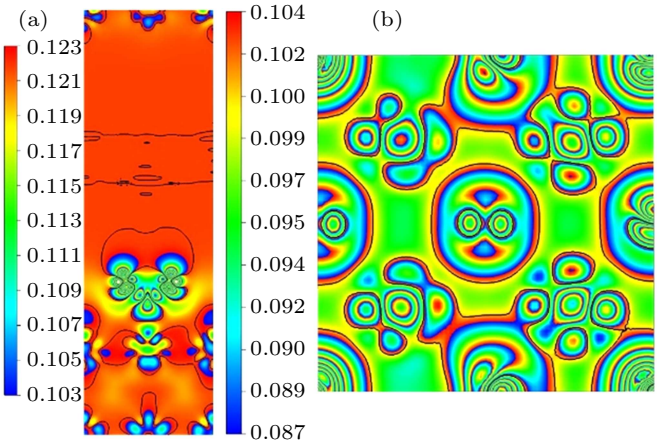


Fig. 9. 2D charge–density difference for (a) T_v-C_4O_7 and (b) T_{p1}-C_2O_8 configurations.

Figure 10 shows the total density of states (TDOS) and partial density of states (PDOS) of the clean δ-Pu(100) surface, and TDOS and PDOS of the most stable adsorption configuration (T_v-C_4O_7) in CO_2-based co-adsorption system. Figure 12(a) shows the corresponding PDOS of T_v-C_4O_7 configuration. From Figs. 10(a) and 10(b) one can see that the peak intensity, position and shape of TDOS change remarkably due to the co-adsorption. The intensity of the first peak increases and turns narrower, while the intensity of the second peak decreases and the peak shape broadens in a range

of −50 eV–42.5 eV. The number of peaks increases, the peak shape broadens and the area increases from −25 eV to −15 eV. In addition, the number and intensity of peaks increase in a range of −12.5 eV–−2.5 eV. However, the peak intensity decreases and the peak shape broadens from −2.5 eV to 2.5 eV. Secondly, as shown in Figs. 10(c), 10(d), and 12(a), the hybridization behavior occurs among C 2s, C 2p, O 2s orbitals, and Pu 6p orbital in a low energy range of −25 eV–−15 eV, moreover, hybridization also occurs among C 2s, C 2p, O 2p orbitals, and Pu 6d, Pu 5f orbitals in a high energy range of −10 eV–−2.5 eV. The intensity of Pu 5f and Pu 6d peaks decreases evidently, and the peak shape broadens in the vicinity of Fermi level (E_F), which indicates that the delocalization of Pu 5f and Pu 6d electrons become stronger, and a small number of Pu 6d and Pu 5f electrons participate in bonding as well.

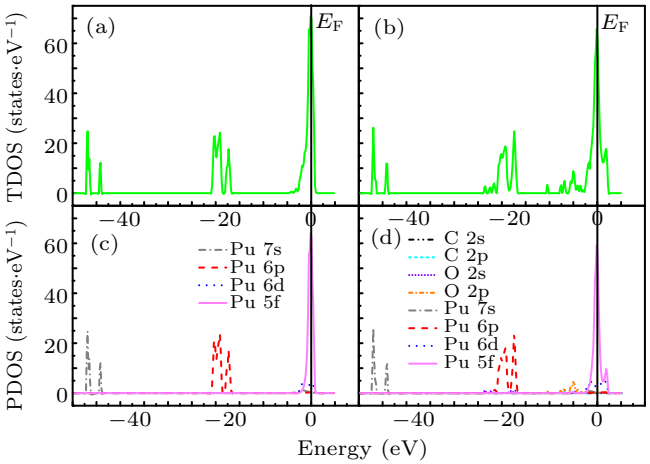


Fig. 10. (a) TDOS of clean δ-Pu (100) surface, (b) TDOS of the most stable configuration (T_v-C_4O_7) in CO_2-based co-adsorption system, (c) PDOS of clean δ-Pu (100) surface, and (d) PDOS of the most stable configuration (T_v-C_4O_7) in CO_2-based co-adsorption system.

Figure 11 displays the TDOS and PDOS of the clean δ-Pu(100) surface, and TDOS and PDOS of the most stable adsorption configuration (T_{p1}-C_2O_8) in O_2-based co-adsorption system. Figure 12(b) shows the corresponding PDOS of T_{p1}-C_2O_8 configuration. From Figs. 11(a) and 11(b), one can see that the peak intensity, position and shape of TDOS change obviously after co-adsorption. The intensity of the first peak increases and the peak shape narrows, while the intensity of the second peak decreases and the peak shape broadens from −50 eV to −42.5 eV. The peak intensity increases, the number of peaks increases, the peak shape broadens and the area increases in a range of −25 eV–−15 eV. Moreover, the number, intensity and area of peaks increase from −12.5 eV to −2.5 eV. The peak intensity decreases, the number of peaks increases, and the peak shape broadens remarkably in a range of −2.5 eV–2.5 eV. As shown in Figs. 11(c), 11(d), and 12(b), the C 2s, C 2p, and O 2s orbitals overlap and hybridize with Pu 6p orbital in a low energy range of −25 eV–−15 eV, furthermore, the C 2s, C 2p, O 2s, and O 2p orbitals overlap and hybridize with Pu 6d and Pu 5f orbitals in a high energy range of −10 eV–2.5 eV. In the vicinity of E_F, the intensity of Pu 5f peak decreases obviously, while the peak intensity decreases slightly and the Pu 6d peak shape broadens, demonstrating that the delocalization of Pu 5f and Pu 6d electrons becomes stronger, and Pu 6d and Pu 5f electrons also take part in bonding, in addition, the Pu 5f electrons make a main contribution.

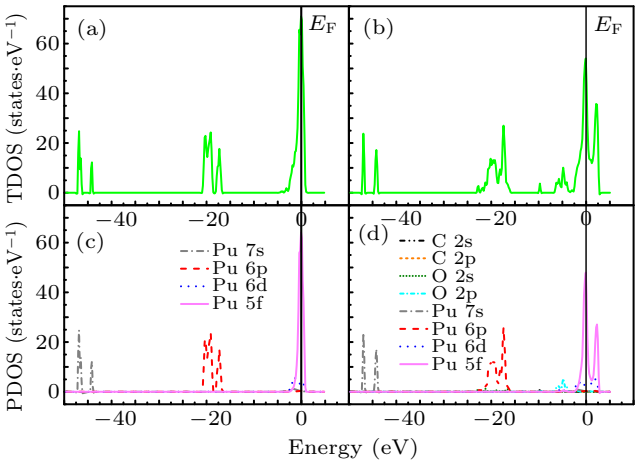


Fig. 11. (a) TDOS of clean δ-Pu (100) surface, (b) TDOS of the most stable configuration (T_{p1}-C_2O_8) in O_2-based co-adsorption system, (c) PDOS of clean δ-Pu (100) surface and (d) PDOS of the most stable configuration (T_{p1}-C_2O_8) in O_2-based co-adsorption system.

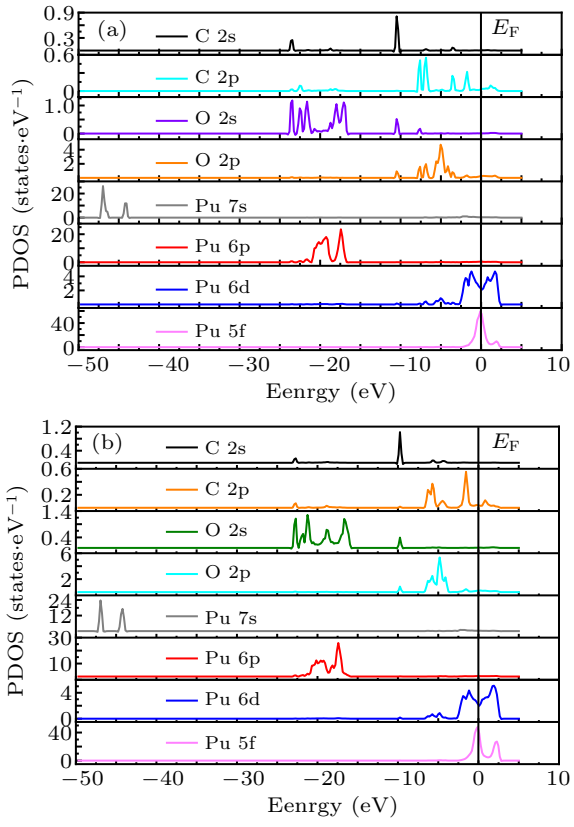


Fig. 12. PDOS of the most stable configuration: (a) T_v-C_4O_7 for CO_2-based system and (b) T_{p1}-C_2O_8 for O_2-based system.

Furthermore, the change of the DOS in T_{p1}-C_2O_8 configuration is greater than that in T_v-C_4O_7 configuration, which indicates that the reaction intensity for T_{p1}-C_2O_8 site is stronger

than that for T_v-C_4O_7 site, and the reaction mechanism among O_2, CO_2 molecules and surface Pu atoms is that the C 2s, C 2p, O 2s, and O 2p orbitals overlap and hybrid with Pu 6p, Pu 6d, and Pu 5f orbitals, the delocalization of Pu 5f and Pu 6d electrons becomes stronger, resulting in a new chemical bonding state, and the O 2s, O 2p, and Pu 5f orbitals make a major contribution.

3.4. Surface work function analysis

Chemically, work function refers to the minimum energy that is required by an electron to escape from a solid surface immediately. It is the energy difference between the vacuum electrostatic potential and the Fermi level at infinity outside the metal, showing the ability of electrons to escape from the metal surface, which reads

$$\Phi = E_{\text{vacuum}} - E_{\text{Fermi}}, \tag{5}$$

where Φ, E_{vacuum}, and E_{Fermi} are the work function, vacuum level, and Fermi level, respectively. The surface work function before and after co-adsorption are listed in Table 3.

Table 3. Surface work function changes ($\Delta\Phi$) of different adsorption configurations. All values are in units of eV.

Configuration	E_{vacuum}	E_{Fermi}	Φ	$\Delta\Phi$
Free surface	6.252	3.299	2.953	–
B_p-C_4O_6	8.054	2.865	5.189	2.236
B_v-CO_6	7.377	3.211	4.166	1.213
H_p-C_4O_6	8.061	2.864	5.198	2.245
H_v-C_4O_6	7.962	2.970	4.992	2.039
T_p-C_4O_7	7.083	3.436	3.647	0.694
T_v-C_4O_7	7.035	3.396	3.639	0.686
B_{v1}-C_2O_8	7.839	3.164	4.674	1.721
B_{p1}-C_1O_9	6.744	3.569	3.175	0.222
B_{p2}-C_2O_8	7.072	3.447	3.625	0.672
B_{v2}-C_1O_9	6.694	3.548	3.146	0.193
H_{v1}-C_4O_8	7.177	3.320	3.857	0.903
H_{v2}-C_2O_7	7.193	3.345	3.848	0.894
H_p-C_2O_6	7.117	3.419	3.698	0.745
T_{p1}-C_2O_8	6.674	3.550	3.125	0.172
T_{p2}-C_1O_9	6.735	3.538	3.197	0.244
T_v-CO_7	6.910	3.545	3.365	0.412

At present, there are no data of experimental work function for δ-Pu. The work function of its neighboring element (uranium) is in a range of 3.63 eV–3.90 eV.[45] The work function of δ-Pu(100) exposed surface, calculated by Wei *et al.*, is 4.365 eV,[46] the work function of δ-Pu(111) slab, calculated by Atta-Fynn *et al.*, is 3.39 eV,[19] and the work function of δ-Pu(020) surface, calculated under non-spin polarization condition, is 3.53 eV.[18] In this work, the calculated work function of δ-Pu(100) surface is 2.9531 eV, and the surface work functions are in a range of 0.686 eV–2.245 eV of the six adsorption states for CO_2-based co-adsorption. What is more, at T_v-C_4O_7 site, the work function increases the least (0.686 eV) with an adsorption energy of −17.296 eV, demonstrating that the energy is lowest and the site is most stable, for this reason, other electrons readily escape from the metal surface and the required energy is least.

The surface work functions of ten adsorption configurations increase from 0.146 eV to 1.721 eV for O_2-based co-adsorption. In addition, the work function of T_{p1}-C_2O_8 configuration is smallest (3.125 eV), and the adsorption energy is also smallest (−23.131 eV), indicating that the energy is lowest and the structure is most stable, so that other electrons readily escape from the metal surface and the required energy is smallest. The increase of surface work function for T_v-C_4O_7 configuration is 0.686 eV, which is larger than that (0.172 eV) for T_{p1}-C_2O_8 site, revealing that the latter is more stable and the energy is lower, thus, the energy needed for electrons to escape from the solid surface is smaller.

4. Conclusions

In this paper, the co-adsorption behaviors of O_2 and CO_2 on the δ-Pu(100) surface are studied by first-principles method. The results show that the O_2 and CO_2 molecules are stably co-adsorbed on δ-Pu(100) surface by C–Pu and O–Pu multi-bondings. Furthermore, the most stable adsorption configurations are T_v-C_4O_7 and T_{p1}-C_2O_8 in CO_2-based and O_2-based cases with the adsorption energy of −17.296 eV and −23.131 eV, respectively, indicating that the structure is more stable for O_2-based adsorption. The O atoms preferentially occupy the hollow and bridge sites after co-adsorption. Bader charge distribution shows that C and O atoms mainly interact with the surface Pu atoms, while the interactions with Pu atoms in the other three low-lying surfaces are weak. The 2D and 3D displays of the charge–density difference show that the chemical binding between C/O and Pu atoms is in ionic state, moreover, the reaction mechanism among O_2 and CO_2 molecules and surface Pu atoms is that the C 2s, C 2p, O 2s, and O 2p orbitals overlap and hybrid with Pu 6p, Pu 6d, and Pu 5f orbitals to produce new chemical bond structure. Importantly, the preferential occupying adsorption of O atoms can promote the adsorption and dissociation of CO_2 molecules obviously. As a result, CO_2 molecules completely dissociate into C+O+O, and the dissociated C atom combine with O atom from O_2 dissociation to produce CO in the O_2-based case, which will inhibit the O_2 from further oxidizing the Pu surface, thereby slowing down the corrosion rate of plutonium-based materials. The finding in this work might shed new light on other relevant actinide-based systems including uranium and americium materials, which have wide applications in nuclear industry. In analogy to the resistance of uranium metal to further oxidation in the atmosphere of CO, indicated by x-ray photoelectron spectroscopy (XPS) method in experiment,[47] the reaction mechanism between CO_2 and “clean” U surface

is that the adsorption of CO_2 on "clean" U metal promotes complete dissociation into uranium dioxide, uranium carbides and free carbon, while CO_2 transforms into carbon, oxygen species, CO_2^{2-} and CO_3^{2-} species.[48]

Acknowledgment

All the work was performed on TianHe-2 platform, Lvliang Cloud Computing Center of China.

References

[1] Haschke J M, Hodges A E and Lucas R L 1987 *J. Less-Common. Met.* **133** 155
[2] S Méot-Reymond and Fournier J M 1996 *J. Alloys Compd.* **232** 119
[3] Almeida T, Cox L E, Ward J W and Naegele J R 1993 *Surf. Sci.* **s287** 141
[4] Stakebake J L, Larson D T and Haschke J M 1993 *J. Alloys Compd.* **202** 251
[5] Oetting F L 1967 *Chem. Rev.* **67** 261
[6] Haschke J M and Ricketts T E 1997 *J. Alloys Compd.* **252** 148
[7] Eriksson O and Cox L E 1991 *Phys. Rev. B* **43** 4590
[8] Huda M N and Ray A K 2005 *Physica B* **366** 95
[9] Huda M N and Ray A K 2004 *Eur. Phys. J. B* **40** 337
[10] Huda M N and Ray A K 2005 *Eur. Phys. J. B* **43** 131
[11] Huda M N and Ray A K 2004 *Physica B* **352** 5
[12] Li G, Lai X C and Sun Y 2005 *Acta Phys. -Chim. Sin.* **21** 686 (in Chinese)
[13] Li G, Lai X C and Sun Y 2005 *J. Atom. Mol. Phys.* **02** 365 (in Chinese)
[14] Atta-Fynn R and Ray A 2007 *Phys. Rev. B* **75** 5112
[15] Atta-Fynn R and Ray A K 2007 *Physica B* **400** 307
[16] Meng D Q, Luo W H, Li G and Chen H C 2009 *Acta Phys. Sin.* **12** 8224 (in Chinese)
[17] Luo W H, Meng D Q, Li G and Chen H C 2008 *Acta Phys. Sin.* **57** 160 (in Chinese)
[18] Wang J and Ray A K 2014 *J. Comput. Theor. Nanosci.* **11** 1710
[19] Atta-Fynn R and Ray A K 2009 *Eur. Phys. J. B* **70** 171
[20] Wei H Y, Song H T, Xiong X L, Wang G Q, Hu R and Luo S Z 2009 *Comput. Appl. Chem.* **26** 913 (in Chinese)
[21] Guo J J, Liu G P and Wei H Y 2013 *Comput. Appl. Chem.* **30** 605 (in Chinese)
[22] Li R S, He B, Xu P, Zhao F T and W F 2014 *Atom. Energ. Sci. Technol.* **48** 43 (in Chinese)
[23] Kresse G and Furthmüller J 1996 *Phys. Rev. B* **54** 11169
[24] Hohenberg P and Kohn W 1964 *Phys. Rev.* **136** 864
[25] Kohn W and Sham L J 1965 *Phys. Rev.* **140** A1133
[26] Blochl P E 1994 *Phys. Rev. B* **50** 17953
[27] Kresse G and Joubert D 1999 *Phys. Rev. B* **59** 1758
[28] Huang G Y, Wang C Y and Wang J T 2009 *J. Phys.: Condens. Matter* **21** 345802
[29] Sui P F, Dai J Q, Zhao Y C and Dai Z H 2019 *Chin. Phys. B* **27** 097311
[30] Wang D W, Wang C Y, Yu T and Liu W Q 2020 *Chin. Phys. B* **29** 043103
[31] Perdew J P, Chevary J A, Vosko S H, Jackson K A, Pederson M R and Singh D J 1992 *Phys. Rev. B* **46** 6671
[32] Perdew J P, Burke K and Ernzerhof M 1996 *Phys. Rev. Lett.* **77** 3865
[33] Monkhorst H J and Pack J D 1976 *Phys. Rev. B* **13** 5188
[34] Payne M C, Teter M P, Allan D C and Arias A 1992 *Rev. Mod. Phys.* **64** 1045
[35] Lide D R 2003 *Crc. Press.* **257** 423
[36] Ogren and Paul J 2002 *J. Chem. Educ.* **79** 117
[37] Li G, Luo W H and Chen H C 2011 *Acta Phys.-Chim. Sin.* **10** 2319 (in Chinese)
[38] Qi C B, Wang T, Wang J T, Tao S H and Qin M A 2020 *Rare. Metal. Mat. Eng.* (accepted, manuscript number: 20200477)
[39] Qi C B, Wang T, Wang J T, Qin M A and Tao S H 2020 *Roy. Soc. Open. Sci.* (under review, manuscript number: RSOS-201395)
[40] Li G, Sun Y, Wang X L, Gao T and Zhu Z H 2003 *Acta Phys.-Chim. Sin.* **4** 356
[41] Green D W and Reedy G T 1978 *Chem. Inform.* **69** 544
[42] Haire R G 1994 *J. Alloy. Compd.* **s213–214** 185
[43] Fu Y B, Wang X L and Zhu Z H 2000 *Eng. Sci.* **2** 59 (in Chinese)
[44] Henkelman G, Amaldsson A and Jonsson H 2006 *Comp. Mater. Sci.* **36** 354
[45] Hao Y G, Eriksson O, Fernando G W and Cooper B R 1993 *Phys. Rev. B* **47** 6680
[46] Wei H Y, Hu R, Xiong X L, Wang G Q, Song H T and Luo S Z 2010 *J. Mol. Sci.* **01** 44 (in Chinese)
[47] Wang X L, Fu Y B and Xie R S 1999 *Atom. Energ. Sci. Technol.* **33** 2 (in Chinese)
[48] Liu K Z, Yu Y, Zou J S, Wu S, Wang X L and Fu Y B 1999 *Chin. Nucl. Sci. Technol. Rep.* **00** 881 (in Chinese)